# Detection of clinically relevant immune checkpoint markers by multicolor flow cytometry

Rachel A. Cunningham, Martha Holland, Emily McWilliams, Frank Stephen Hodi, Mariano Severgnini*

Department of Medical Oncology, Center for Immuno-Oncology, Dana-Farber Cancer Institute, 450 Brookline, Ave Mayer Building 305, Boston, MA 02215, USA

*Corresponding author: Mariano Severgnini, Email: Mariano_severgnini@dfci.harvard.edu

## ABSTRACT

As checkpoint inhibitor immunotherapies gain traction among cancer researchers and clinicians, the need grows for assays that can definitively phenotype patient immune cells. Herein, we present an 8-color flow cytometry panel for lineage and immune checkpoint markers and validate it using healthy human donor peripheral blood mononuclear cells (PBMCs). Flow cytometry data was generated on a BD LSR Fortessa and supported by Luminex multiplex soluble immunoassay. Our data showed significant variation between donors at both baseline and different stages of activation, as well as a trend in increasing expression of checkpoint markers on stimulated CD4$^+$ and CD8$^+$ T-cells with time. Soluble immune checkpoint quantification assays revealed that LAG-3, TIM-3, CTLA-4, and PD-1 soluble isoforms are upregulated after stimulation. This 8-color flow cytometry panel, supported here by soluble immunoassay, can be used to identify and evaluate immune checkpoints on T-lymphocytes in cryopreserved human PBMC samples. This panel is ideal for characterizing checkpoint expression in clinical samples for which cryopreservation is necessary.

**Keywords:** checkpoint markers, flow cytometry, immuno-phenotype, immunotherapy

## INTRODUCTION

Checkpoint inhibitor therapies are a class of drugs that inhibit immune regulatory proteins to induce an endogenous immune response against tumor cells.

Several currently approved checkpoint inhibitors target programmed cell death protein 1 (PD-1) [1], an inhibitory protein expressed on exhausted T-lymphocytes [2,3]. Other checkpoint immunotherapies block cytotoxic T-lymphocyte-associated protein 4 (CTLA-4) [4,5] a CD28 homolog that competitively binds CD80 and CD86 to inhibit the immune effector function of T-cells [6]. Clinical interest in checkpoint inhibitor therapies continue to grow as new indications and mechanisms are discovered.

Since the first checkpoint inhibitor ipilimumab (an anti-CTLA-4 monoclonal antibody), was approved in 2011 [7], five additional checkpoint-blocking antibody drugs have been approved to treat a variety of solid tumors [8-11].

Next-generation therapies target other immune checkpoints such as inducible T-cell costimulatory (ICOS) [12], T-cell immunoglobulin and mucin domain 3 (TIM-3) [13], and lymphocyte activation gene 3 (LAG-3) [14,15]. These have attracted interest in recent years due to successes in animal models [16,17] and clinical trials [18].

As these therapies emerge as valuable new tools in cancer treatment, it becomes necessary to develop reliable methods of predicting and monitoring immune responses to these drugs. While some previously validated flow cytometry panels endeavor to characterize immune cell subsets [19], or define the immune status of cell subsets [20], this panel is specialized to measure the expression of several clinically relevant immune checkpoints expressed on T-cells.

By ascertaining that flow panels reveal the expected immunophenotypes in healthy human donor cells without excessive artifacts from fluorescent spillover and compensation [21], the panel validation performed here enables the informed analysis of clinical samples using the panel in question [22,23].

This paper validates an 8-color flow cytometry panel that allows for the detection of several clinically relevant checkpoint biomarkers

including CTLA-4, PD-1, LAG-3, TIM-3, and ICOS in human T-lymphocytes. The panel is optimized for cryopreserved PBMCs and is therefore applicable for immunotherapy clinical samples.

## MATERIALS AND METHODS

### Isolation of donor PBMCs

Whole blood samples were collected from six healthy human donors in accordance with the protocol approved by the Institutional Review Board of Brigham and Women's Hospital. PBMCs were isolated from whole blood within 6 h of collection and processed according to the methods described by Holland *et al*. [24].

### Cell culture & stimulation

Cells were removed from liquid nitrogen storage and thawed in a 37°C water bath. Upon thawing, cells were pipetted out of the cryovial into 12 ml of warmed RPMI (ThermoFisher Scientific, Waltham, MA, USA) supplemented with 10% FBS and 1× antimycotic-antifungal (ThermoFisher Scientific).

Cell suspension aliquots were filled to 15 ml with supplemented RPMI, counted, and then centrifuged at 272RCFs for 5 min. All subsequent centrifugations were done at 4°C with acceleration set to 7 and deceleration set to 7, with the centrifuge brake off.

Supernatant was discarded and cells were resuspended in RPMI to 5 million cells/ml. 2 ml of cell suspension was aliquoted into one well of each of three 6-well plates. This volume was brought up to 5 ml with RPMI.

For the 48 h stimulation condition, CD3/CD28 Dynabeads (ThermoFisher Scientific) were added in a ratio of 1 million beads per 10 million cells. Plates were placed in an incubator at 37°C 5% $CO_2$ overnight.

Twenty-four hours after plating, one plate was removed for the 24 h stimulation condition and supplemented with Dynabeads at 1 million beads per 10 million cells. The remaining plate was allowed to incubate without stimulation for the whole 48 h incubation, as described by Patel *et al*. [21].

After 48 h from initial plating, 500 μl of media was removed from each well and placed in 1.7 ml Eppendorf tubes. These tubes were cen-trifuged at 9615RCFs for 5 min and 450 μl of the resulting supernatant was pipetted into a deep well 96-well plate (ThermoFisher Scientific) to be stored at −80°C for later use in the soluble immunoassay.

The remaining cell suspensions were moved from plates to 15 ml conical tubes, and Dynabeads were removed *via* magnet.

### Flow cytometry staining

Cells were placed on ice, then counted and centrifuged for 5 min at 272RCFs. Pellets were resuspended at 10 million cells/ml, and aliquoted into a 96 well v-bottom plate at 1.5 million cells per well.

After washing with 150 μl PBS per well, cells were stained with 150 μl Zombie Near IR fixable viability cell dye (Biolegend, San Diego, CA, USA) at a dilution of 1:2500 in PBS, and left on ice to incubate for 18 min in the dark.

The plate was then centrifuged at 757RCFs for 3 min, and cells washed again with PBS. Cells were then incubated with FcR blocking reagent (Miltenyi Biotec, Bergisch Gladbach, Germany) diluted 1:625 in FACS buffer (PBS, 2.5% FBS) for 18 min on ice in the dark. Following FcR block, cells were stained in 100 μl total stain volume with predetermined antibody volumes (**Table 1**).

Cells were then washed twice with FACS buffer and fixed in 2% paraformaldehyde (EK Industries, Joliet, IL, USA) before being stored at 4°C overnight and acquired the next day on a BD LSR Fortessa analyzer (BD Biosciences, San Jose, CA, USA).

Antibody staining concentrations were pre-determined in titration experiments to show the best separation between positive and negative populations [21]. The emission spectrum of APC-Cy7 overlaps almost completely with that of Zombie NIR, and so can be used to tag cells to be gated out—in this case, CD56^{+} cells. Averaged voltages for FSC-A and SSC-A were 280.00 and 181.67 respectively.

### Flow cytometry

Cells were diluted with 50 μl PBS before acquisition. 1-peak Rainbow Beads (Biolegend) were used to inform voltage settings. Compensation controls were established based on auto-compensation using single color control ultra-comp beads (ThermoFisher Scientific). Voltages were set on each parameter (**Table 1**) to ensure minimal spillover between fluorophores.

**Table 1. Antibodies used for immune checkpoint panel development.**

| Antibody | Fluorophore | Clone | Vendor | Catalogue # | Volume Antibody in well (μl) | Voltage (averaged) | Marker function |
|---|---|---|---|---|---|---|---|
| CD3 | PE/Cy7 | UCHT1 | eBioscience (San Diego, CA, USA) | 25-0038-42 | 1.50 | 359.00 | Lineage |
| CD4 | FITC | OKT4 | eBioScience | 11-0048-42 | 0.30 | 386.67 | Lineage |
| CD8 | APC | BW135/80 | Miltenyi Biotec | 130-091-076 | 1.25 | 525.00 | Lineage |
| PD-1 | BV510 | EH12.2H7 | Biolegend | 329932 | 5.00 | 395.00 | Checkpoint |
| CTLA-4 | PE | L3D10 | Biolegend | 349906 | 2.50 | 353.33 | Checkpoint |
| ICOS | BV650 | DX29 | BD Biosciences | 563832 | 3.00 | 461.67 | Checkpoint |
| TIM-3 | BV421 | F382E2 | Biolegend | 345008 | 7.50 | 325.00 | Checkpoint |
| LAG-3 | PerCP-Cy5.5 | 11c3c65 | Biolegend | 369312 | 5.00 | 496.67 | Checkpoint |
| CD56 | APC-Cy7 | HCD56 | Biolegend | 318332 | 7.50 | -- | Lineage (NK cell exclusion) |
| Viability | Zombie NIR | -- | Biolegend | 423105 | 0.06 | 456.67 | Dead cell exclusion |

The resulting FCS files were analyzed using FlowJo (FlowJo LLC, Ashland, OR, USA). All gating was based on unstained and fluorescence minus one (FMO) controls. Two FMO controls were used; one missing anti-PD-1-BV510 and anti-CTLA-4-PE (FMO1), and one missing anti-ICOS-BV650, anti-TIM-3-BV421, and anti-LAG-3-PerCP-Cy5.5 (FMO2). FMO cell populations were comprised of non-stimulated, 24 h stimulated, and 48 h stimulated cells combined in equal measure. Gating was performed on contour plots and pseudocolor dot plots in FlowJo (**Fig. S1**). CD56$^+$ cells such as natural killer and natural killer T-cells were excluded from further analysis *via* the live cell gating.

Graphs were created with GraphPad Prism version 8.0 (GraphPad Software, La Jolla, CA, USA).

## Soluble checkpoint detection assay

Reserved cell culture supernatant was stored at −80°C. After thawing, 2-fold diluted supernatant was analyzed for all non-stimulated and 48 h stimulated samples across all replicates. Diluted supernatant was processed according to the protocol provided with the ProcartaPlex™ Multiplex Immunoassay for Human Immuno-Oncology Checkpoint Marker Panel (ThermoFisher Scientific). Prepared samples were read on a Luminex FLEXMAP 3D System (Luminex Corporation, Austin, TX, USA). Supernatant was used to quantify soluble LAG-3, TIM-3, CTLA-4, and PD-1.

Voltages were set such that the negative population was on scale and the positive population fell at or above $10^4$ median fluorescence intensities (MFIs). The compensation matrix was adjusted in FlowJo to better represent the compensated data (**Table S1**).

Gating for immune checkpoints was performed on populations already gated on Lymphocytes/singlets/live cells/CD3$^+$/CD4$^+$ or CD8$^+$ (**Fig. 1**).

Gating for checkpoints was controlled by FMOs and unstained controls. All gates were conserved across samples for each individual donor.

Both CD4$^+$ and CD8$^+$ populations were evaluated for immune checkpoints (**Fig. 2**). Checkpoint proteins showed a general increase in expression correlated with length of T-cell stimulation in culture. Average fold changes of checkpoint expression in both 24 h and 48 h stimulated cells showed a marked increase over non-stimulated cells (**Fig. 3**). Fold changes ranged from 1.08-fold average decreases in PD-1 expression (Donor B, 24 h stimulated CD8$^+$ cells) to 57.2-fold average increases in LAG-3 expression (Donor E, 24 h stimulated CD8$^+$ cells). There was a great deal of differential expression between donors (**Table 2**), with some donors showing much higher baseline levels of certain checkpoint markers such as PD-1 in Donor A for both CD4$^+$ and CD8$^+$ cells. Further, each donor showed different rates and levels of activation that were not necessarily conserved across all checkpoint markers. Generally, CD4$^+$ populations demonstrated more predictable linear increases in checkpoint expression, while CD8$^+$ populations were slightly less likely to follow this pattern.

## RESULTS
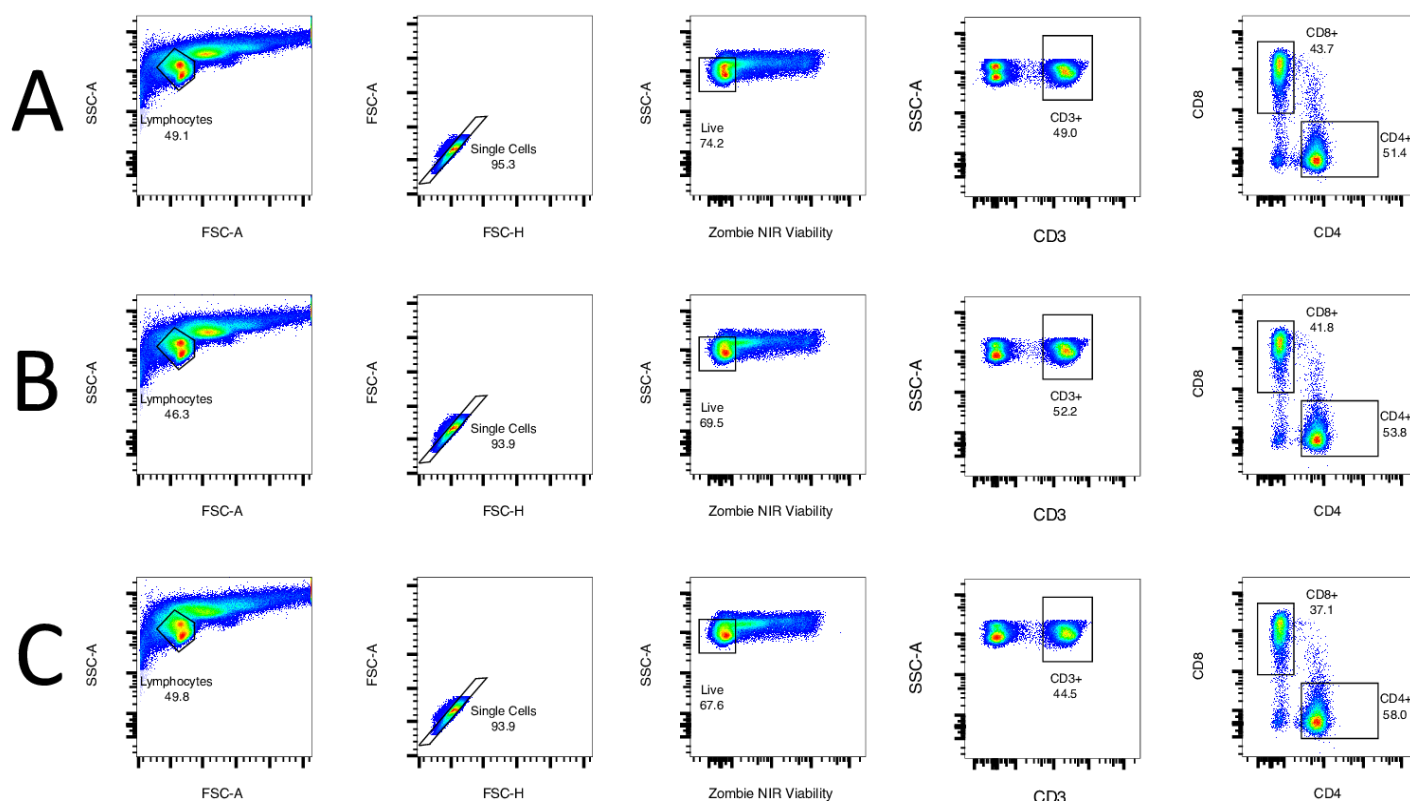


**Figure 1. Example lineage gating strategy using pseudocolor dot plots.** Shown are example hierarchies from the non-stimulated sample (A), the 24 h stimulated sample (B) and the 48 h stimulated sample from donor C (C). Figure generated using FlowJo.
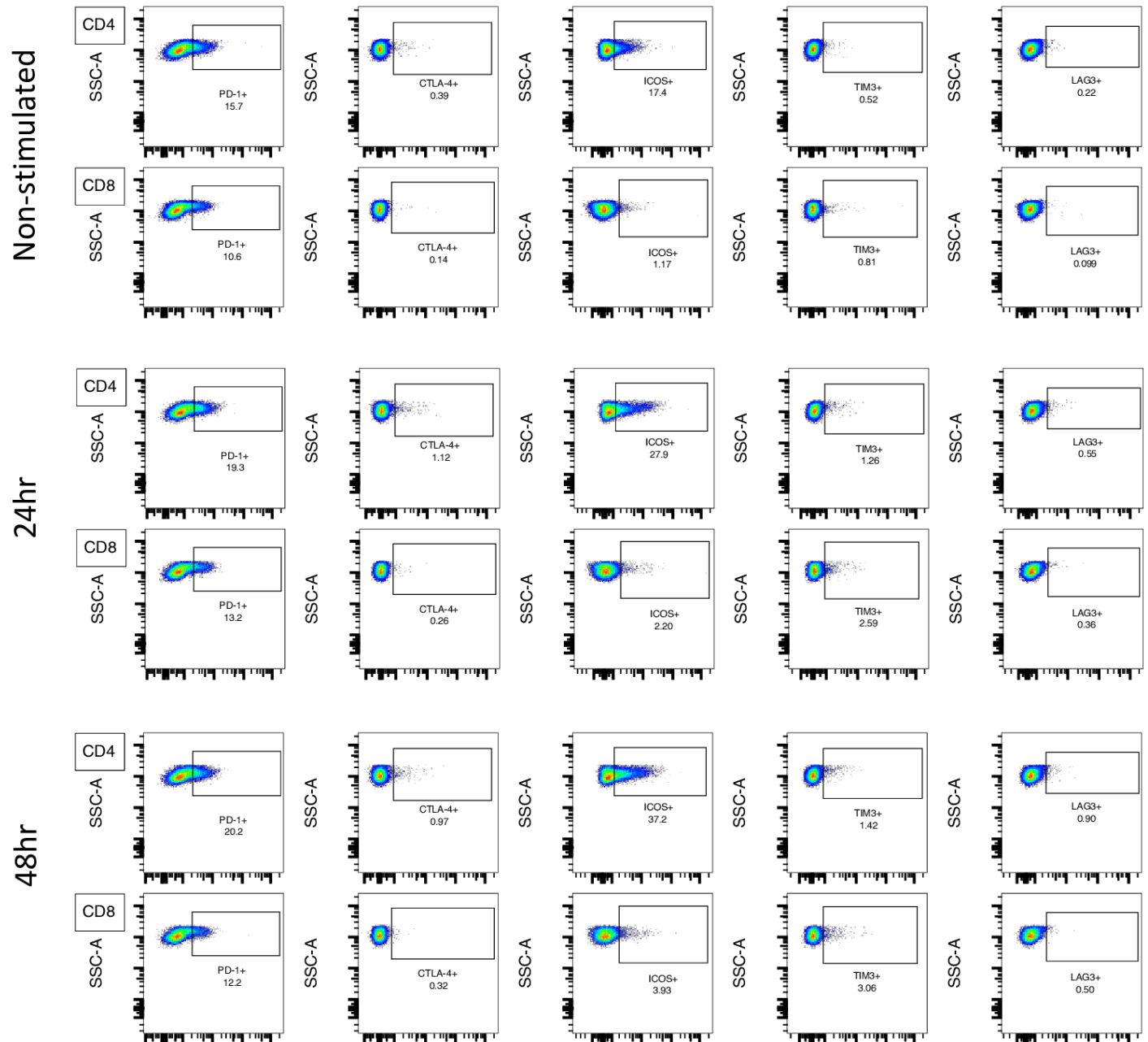
**Figure 2. Example functional marker gating strategy for CD4+ and CD8+ T-lymphocytes.** Dot plots show Lymphocyte/singlet/live/CD3+/CD4+ or CD8+ populations of cells from the non-stimulated sample, 24 h stimulated, and 48 h stimulated sample from donor C. Figure was generated using FlowJo.

Soluble checkpoint multiplex assay revealed that all donors upregulated expression of TIM-3, CTLA-4, LAG-3, and PD-1 after 48 h stimulation (**Fig. 4**). Since the soluble forms of TIM-3, PD-1, and LAG-3 are formed by proteolytic cleavage from the membrane [25,26], this confirms the flow cytometry finding that all three were upregulated with T-cell stimulation. Soluble CTLA-4 is secreted rather than shed from the membrane, but upregulation of soluble CTLA-4 is associated with CD4+ T-cell activation [27], indicating that the cells were successfully stimulated. Results from the Luminex assay therefore confirm those of the flow cytometric analysis.

## DISCUSSION

This panel enables the detection of five extracellular immune checkpoint markers on T-lymphocytes. The six healthy donors assayed in this experiment demonstrate checkpoint expression consistent with expectation—that is, upregulation of both membrane-bound and soluble immune checkpoints with prolonged T-cell stimulation.

Though the protocol shown here demonstrates a valid and reproducible procedure for stimulating healthy donor PBMCs for detection of T-cell markers, our data also highlight the non-trivial inter-donor variation in response to CD3/CD28 stimulation. For clinical samples, careful

statistical analysis should be planned to control for such variation, as was recently described by Rodig *et al.* [28].

The presence and upregulation of checkpoint markers was determined by flow cytometry and Luminex immunoassay. The panel developed here therefore provides a means of detecting varying levels of membrane-bound checkpoint proteins, as might occur in clinical samples.

Our data validate an 8-color antibody panel that is capable of identifying clinically relevant immune checkpoint markers in CD4$^+$ and CD8$^+$ T-lymphocytes isolated from cryopreserved human PBMCs. This is highly applicable to the field of immuno-oncology, where the detection of immune checkpoints is critical to both identifying potential biomarkers and predicting patient response potential.
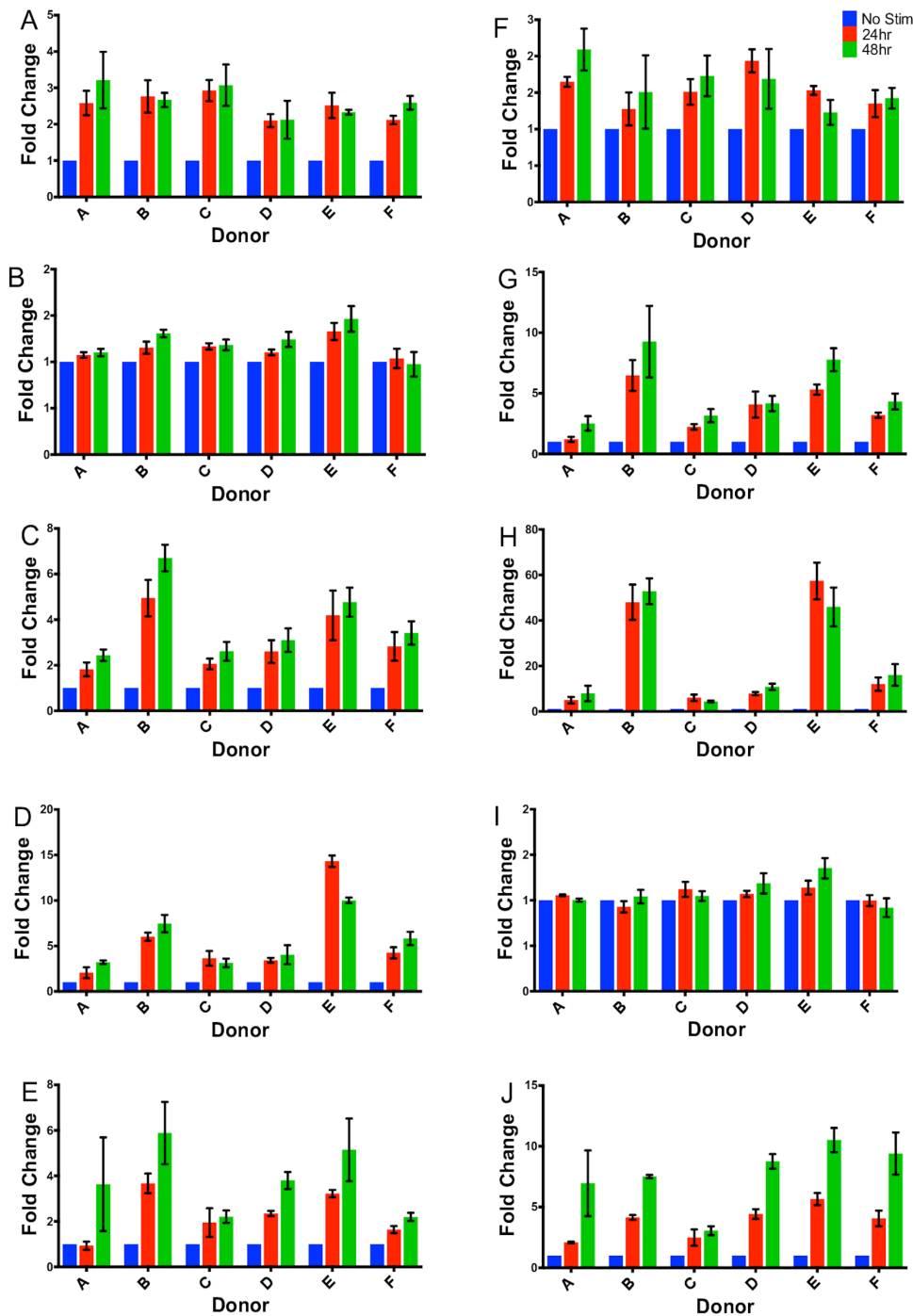


**Figure 3. Comparative changes in checkpoint expression in CD4$^+$ and CD8$^+$ T-lymphocytes represented as fold change in percent of parent population.** All cells were gated on Lymphocytes/singlets/live/CD3$^+$/CD4$^+$ or CD8$^+$. Graphs represent checkpoint gating on CD4$^+$ cells for PD-1 (A), CTLA-4 (B), ICOS (C), TIM-3 (D), and LAG-3 (E), and on CD8$^+$ cells for PD-1 (F), CTLA-4 (G), ICOS (H), TIM-3 (I), and LAG-3 (J). Error bars represent standard error of the mean. No statistical analysis was performed on this data, and conclusions were based on general trends. Figures were generated using GraphPad Prism.
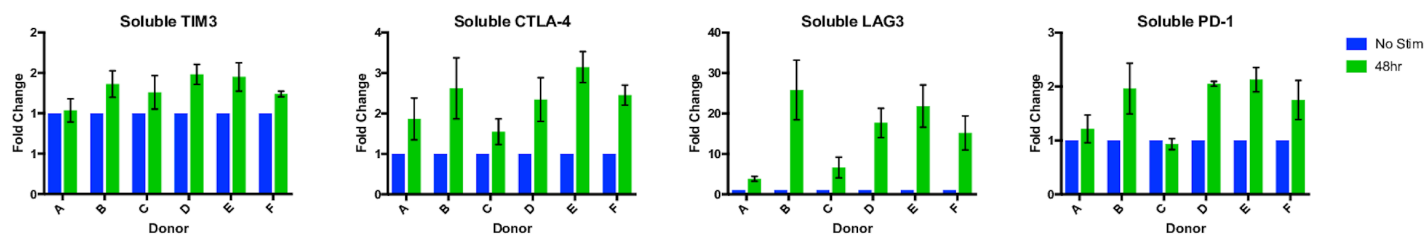
**Figure 4. Average fold change in soluble checkpoint supernatant concentration between non-stimulated and 48 h stimulated cells as measured by Luminex assay.** TIM-3, CTLA-4, LAG-3, and PD-1 soluble isoforms showed upregulation following 48 h stimulation for all donors. Error bars represent standard error of the mean. No statistical analysis was performed on this data, and conclusions were based on general trends Figure generated using GraphPad Prism.

**Table 2. Averaged percent of parent populations positive for selected checkpoint markers in non-stimulated, 24 h, and 48 h stimulated populations in CD4⁺ and CD8⁺ cells.**

| CD4⁺ | | | | | | | | | | | | | | | |
|---|---|---|---|---|---|---|---|---|---|---|---|---|---|---|
| | PD-1⁺ | | | CTLA-4⁺ | | | ICOS⁺ | | | TIM-3⁺ | | | LAG-3⁺ | | |
| | No stim | 24 h | 48 h | No stim | 24 h | 48 h | No stim | 24 h | 48 h | No stim | 24 h | 48 h | No stim | 24 h | 48 h |
| A | 37.37 | 40.10 | 41.03 | 0.67 | 1.69 | 2.07 | 13.21 | 22.00 | 30.60 | 0.58 | 0.51 | 2.48 | 0.54 | 0.91 | 1.65 |
| B | 10.57 | 12.25 | 13.90 | 0.24 | 0.65 | 0.63 | 3.55 | 15.50 | 22.07 | 0.16 | 0.60 | 0.94 | 0.34 | 2.14 | 2.42 |
| C | 16.73 | 19.60 | 19.60 | 0.37 | 1.08 | 1.12 | 9.43 | 17.53 | 22.40 | 0.69 | 1.13 | 1.46 | 0.41 | 1.49 | 1.19 |
| D | 11.27 | 12.43 | 14.00 | 0.28 | 0.56 | 0.53 | 10.44 | 22.47 | 27.80 | 0.20 | 0.48 | 0.78 | 0.21 | 0.67 | 0.69 |
| E | 4.49 | 5.96 | 6.51 | 0.24 | 0.61 | 0.57 | 4.25 | 14.10 | 17.73 | 0.22 | 0.71 | 1.10 | 0.22 | 3.18 | 2.22 |
| F | 12.17 | 12.43 | 11.62 | 0.29 | 0.61 | 0.77 | 6.38 | 14.64 | 18.90 | 0.20 | 0.32 | 0.44 | 0.35 | 1.32 | 1.83 |
| CD8⁺ | | | | | | | | | | | | | | | |
| | PD-1⁺ | | | CTLA-4⁺ | | | ICOS⁺ | | | TIM-3⁺ | | | LAG-3⁺ | | |
| | No stim | 24 h | 48 h | No stim | 24 h | 48 h | No stim | 24 h | 48 h | No stim | 24 h | 48 h | No stim | 24 h | 48 h |
| A | 52.77 | 55.73 | 52.90 | 0.26 | 0.42 | 0.54 | 1.02 | 1.17 | 2.60 | 1.32 | 2.73 | 9.95 | 0.42 | 2.49 | 3.45 |
| B | 15.07 | 14.03 | 15.67 | 0.18 | 0.21 | 0.22 | 0.15 | 1.00 | 1.46 | 0.38 | 1.55 | 2.84 | 0.09 | 4.40 | 4.39 |
| C | 11.60 | 13.00 | 12.10 | 0.24 | 0.35 | 0.39 | 0.77 | 1.63 | 2.41 | 0.97 | 2.20 | 2.91 | 0.36 | 2.37 | 1.54 |
| D | 18.10 | 19.27 | 21.17 | 0.19 | 0.36 | 0.29 | 0.56 | 2.03 | 2.37 | 0.51 | 2.19 | 4.36 | 0.23 | 1.89 | 2.40 |
| E | 6.86 | 7.77 | 9.20 | 0.18 | 0.27 | 0.22 | 0.26 | 1.35 | 2.19 | 0.50 | 2.82 | 5.33 | 0.18 | 10.89 | 8.94 |
| F | 11.60 | 11.57 | 10.69 | 0.23 | 0.28 | 0.30 | 0.19 | 0.60 | 0.81 | 0.30 | 1.12 | 2.57 | 0.21 | 2.57 | 3.49 |

## References

1. Sasaki H (1989) Subpial glial limiting membrane of the cat spinal cord visualized by scanning electron microscopy. Anat Embryol (Berl) 179: 533-540. PMID: 2751115

2. Freeman GJ, Long AJ, Iwai Y, Bourque K, Chernova T, et al. (2000) Engagement of the PD-1 immunoinhibitory receptor by a novel B7 family member leads to negative regulation of lymphocyte activation. J Exp Med 192: 1027-1034. PMID: 11015443

3. Jin HT, Ahmed R, Okazaki T (2010) Role of PD-1 in regulating T-cell immunity. Curr Top Microbiol Immunol 350: 17-37. doi: 10.1007/82_2010_116. PMID: 21061197

4. Hodi FS, O'Day SJ, McDermott DF, Weber RW, Sosman JA, et al. (2010) Improved survival with ipilimumab in patients with metastatic melanoma. N Engl J Med 363: 711-723. doi: 10.1056/NEJMoa1003466. PMID: 20525992

5. Lipson EJ, Drake CG (2011) Ipilimumab: an anti-CTLA-4 antibody for metastatic melanoma. Clin Cancer Res 17: 6958-6962. doi: 10.1158/1078-0432.CCR-11-1595. PMID: 21900389

6. Melero I, Hervas-Stubbs S, Glennie M, Pardoll DM, Chen L (2007) Immunostimulatory monoclonal antibodies for cancer therapy. Nat Rev Cancer 7: 95-106. doi: 10.1038/nrc2051. PMID: 17251916

7. Wolchok JD, Hodi FS, Weber JS, Allison JP, Urba WJ, et al. (2013) Development of ipilimumab: a novel immunotherapeutic approach for the treatment of

advanced melanoma. Ann N Y Acad Sci 1291: 1-13. doi: 10.1111/nyas.12180. PMID: 23772560

8. Dine J, Gordon R, Shames Y, Kasler MK, Barton-Burke M (2017) Immune checkpoint inhibitors: An innovation in immunotherapy for the treatment and management of patients with cancer. Asia Pac J Oncol Nurs 4: 127-135. doi: 10.4103/apjon.apjon_4_17. PMID: 28503645

9. Massard C, Gordon MS, Sharma S, Rafii S, Wainberg ZA, et al. (2016) Safety and Efficacy of Durvalumab (MEDI4736), an Anti-Programmed Cell Death Ligand-1 Immune Checkpoint Inhibitor, in Patients With Advanced Urothelial Bladder Cancer. J Clin Oncol 34: 3119-3125. doi: 10.1200/JCO.2016.67.9761. PMID: 27269937

10. Rosenberg JE, Hoffman-Censits J, Powles T, van der Heijden, MS, Balar AV, et al. (2016) Atezolizumab in patients with locally advanced and metastatic urothelial carcinoma who have progressed following treatment with platinum-based chemotherapy: a single-arm, multicentre, phase 2 trial. Lancet 387: 1909-1920. doi: 10.1016/S0140-6736(16)00561-4. PMID: 26952546

11. Kaufman HL, Russell J, Hamid O, Bhatia S, Terheyden P, et al. (2016) Avelumab in patients with chemotherapy-refractory metastatic Merkel cell carcinoma: a multicentre, single-group, open-label, phase 2 trial. Lancet Oncol 17: 1374-1385. doi: 10.1016/S1470-2045(16)30364-3. PMID: 27592805

12. Amatore F, Gorvel L, Olive D (2018) Inducible Co-Stimulator (ICOS) as a potential therapeutic target for anti-cancer therapy. Expert Opin Ther Targets 22: 343-351. doi: 10.1080/14728222.2018.1444753. PMID: 29468927

13. Du W, Yang M, Turner A, Xu C, Ferris RL, et al. (2017) TIM-3 as a Target for Cancer Immunotherapy and Mechanisms of Action. Int J Mol Sci 18: 645. doi: 10.3390/ijms18030645. PMID: 28300768

14. Goldberg MV, Drake CG (2010) LAG-3 in cancer immunotherapy. Curr Top Microbiol Immunol 344: 269-278. doi: 10.1007/82_2010_114. PMID: 21086108

15. Andrews LP, Marciscano AE, Drake CG, Vignali DAA (2017) LAG3 (CD223) as a cancer immunotherapy target. Immunol Rev 276: 80-96. doi: 10.1111/imr.12519. PMID: 28258692

16. Shimizu T, Fuchimoto Y, Okita H, Fukuda K, Kitagawa Y, et al. (2018) A curative treatment strategy using tumor debulking surgery combined with immune checkpoint inhibitors for advanced pediatric solid tumors: An in vivo study using a murine model of osteosarcoma. J Pediatr Surg 53: 2460-2464. doi: 10.1016/j.jpedsurg.2018.08.023. PMID: 30266483

17. Fan X, Quezada SA, Sepulveda MA, Sharma P, Allison JP (2014) Engagement of the ICOS pathway markedly enhances efficacy of CTLA-4 blockade in cancer immunotherapy. J Exp Med 211: 715-725. doi: 10.1084/jem.20130590. PMID: 24687957

18. Ascierto PA, Melero I, Bhatia S, Bono P, Sanborn RE, et al. (2017) Initial efficacy of anti-lymphocyte activation gene-3 (anti–LAG-3; BMS-986016) in combination with nivolumab (nivo) in pts with melanoma (MEL) previously treated with anti–PD-1/PD-L1 therapy. J Clin Oncol 35: 9520-9520. doi: 10.1200/JCO.2017.35.15_suppl.9520.

19. Rühle PF, Fietkau R, Gaipl US, Frey B (2016) Development of a Modular Assay for Detailed Immunophenotyping of Peripheral Human Whole Blood Samples by Multicolor Flow Cytometry. Int J Mol Sci 17: 1316. doi: 10.3390/ijms17081316. PMID: 27529227

20. Donaubauer A, Rühle PF, Becker I, Fietkau R, Gaipl US, et al. (2019) One-Tube Multicolor Flow Cytometry Assay (OTMA) for Comprehensive Immunophenotyping of Peripheral Blood. Methods Mol Biol 1904: 189-212. doi: 10.1007/978-1-4939-8958-4_8. PMID: 30539471

21. Patel T, Cunningham A, Holland M, Daley J, Lazo S, et al. (2017) Development of an 8-color antibody panel for functional phenotyping of human CD8+ cytotoxic T cells from peripheral blood mononuclear cells. Cytotechnology 70: 1-11. doi: 10.1007/s10616-017-0106-3. PMID: 28551826

22. Sridharan V, Margalit DN, Lynch SA, Severgnini M, Zhou J, et al. (2016) Definitive chemoradiation alters the immunologic landscape and immune checkpoints in head and neck cancer. Br J Cancer 115: 252-260. doi: 10.1038/bjc.2016.166. PMID: 27380136

23. Ben-Ami E, Barysauskas CM, Solomon S, Tahlil K, Malley R, et al. (2017) Immunotherapy with single agent nivolumab for advanced leiomyosarcoma of the uterus: Results of a phase 2 study. Cancer 123: 3285-3290. doi: 10.1002/cncr.30738. PMID: 28440953

24. Holland M, Cunningham R, Seymour L, Kleinsteuber K, Cunningham A, et al. (2018) Separation, banking, and quality control of peripheral blood mononuclear cells from whole blood of melanoma patients. Cell Tissue Bank 19: 783-790. doi: 10.1007/s10561-018-9734-x. PMID: 30377864

25. Clayton KL, Douglas-Vail MB, Nur-ur Rahman, A.K.M. , Medcalf KE, Xie IY, et al. (2015) Soluble T cell immunoglobulin mucin domain 3 is shed from CD8+ T cells by the sheddase ADAM10, is increased in plasma during untreated HIV infection, and correlates with HIV disease progression. J Virol 89: 3723-3736. doi: 10.1128/JVI.00006-15. PMID: 25609823

26. Zhu X, Lang J (2017) Soluble PD-1 and PD-L1: predictive and prognostic significance in cancer. Oncotarget 8: 97671-97682. doi: 10.18632/oncotarget.18311. PMID: 29228642

27. Esposito L, Hunter KMD, Clark J, Rainbow DB, Stevens H, et al. (2014) Investigation of soluble and transmembrane CTLA-4 isoforms in serum and microvesicles. J Immunol 193: 889-900. doi: 10.4049/jimmunol.1303389. PMID: 24928993

28. Rodig SJ, Gusenleitner D, Jackson DG, Gjini E, Giobbie-Hurder A, et al. (2018) MHC proteins confer differential sensitivity to CTLA-4 and PD-1 blockade in untreated metastatic melanoma. Sci Transl Med 10: doi: 10.1126/scitranslmed.aar3342. PMID: 30021886

## Supplementary information

**Figure S1**. Example gating strategy of cells using pseudocolor dot plot and contour plots.

**Figure S2**. Dot plots of unstained, FMO1, and FMO2 lineage gating.

**Figure S3**. Dot plots of FMO1, and FMO2 checkpoint expression.

**Table S1**. Averaged compensation matrix for panel.

Supplementary information of this article can be found online at http://www.jbmethods.org/jbm/rt/suppFiles/283.